HHS Public Access

Author manuscript

Cell Mol Neurobiol. Author manuscript; available in PMC 2023 October 01.

Published in final edited form as:

Cell Mol Neurobiol. 2022 October ; 42(7): 2187–2204. doi:10.1007/s10571-021-01088-1.

MACF1 involved in the 1p34.2p34.3 microdeletion syndrome is essential in cortical progenitor polarity and brain integrity

Minhan Ka[#1], **Jeffrey J. Moffat**[#2], **Woo-Yang Kim**[3,*]

[1]Research Center for Substance Abuse Pharmacology, Korea Institute of Toxicology, Daejeon 34114, Republic of Korea

[2]Developmental Neuroscience, University of Nebraska Medical Center, Omaha, NE 68198, USA

[3]Department of Biological Sciences, Kent State University, Kent, OH 44242, USA

[#] These authors contributed equally to this work.

Abstract

1p34.2p34.3 deletion syndrome is characterized by an increased risk for autism. *Microtubule Actin Crosslinking Factor 1* (*MACF1)* is one candidate gene for this syndrome. It is unclear, however, how *MACF1* deletion is linked to brain development and neurodevelopmental deficits. Here we report on *Macf1* deletion in the developing mouse cerebral cortex, focusing on radial glia polarity and morphological integrity, as these are critical factors in brain formation. We found that deleting *Macf1* during cortical development resulted in double cortex/subcortical band heterotopia as well as disrupted cortical lamination. *Macf1*-deleted radial progenitors showed increased proliferation rates compared to control cells but failed to remain confined within their defined proliferation zone in the developing brain. The overproliferation of *Macf1*-deleted radial progenitors was associated with elevated cell cycle speed and re-entry. Microtubule stability and actin polymerization along the apical ventricular area were decreased in the *Macf1* mutant cortex. Correspondingly, there was a disconnection between radial glial fibers and the apical and pial

[*]**Correspondence to:** Woo-Yang Kim, Ph.D., wkim2@kent.edu, Phone: 330-672-7888.

Author contribution

M.K., J.J.M., and W.K. conceived, designed, performed, and analyzed the experiments. M.K. performed and analyzed the majority of the imaging experiments. J.J.M. performed and analyzed the majority of the behavior experiments. M.K., J.M., and W.K. wrote the paper. W.K. supervised the work.

Conflicts of interest/ Competing interests

Authors declare no competing financial interests.

Declarations

Availability of data and material

Data and materials will be available depending on request and availability.

Code availability

Not applicable.

Ethics approval

Mice were handled in accordance with the animal protocol approved by the Institutional Animal Care and Use Committees (IACUC) at the University of Nebraska Medical Center and Kent State University. All experimental procedures met National Institutes of Health guidelines for the care and use of laboratory animals.

Consent to participate

Not applicable.

Consent for publication

Not applicable.

surfaces. Finally, we observed that *Macf1*-mutant mice exhibited social deficits and aberrant emotional behaviors. Together, these results suggest that MACF1 plays a critical role in cortical progenitor proliferation and localization by promoting glial fiber stabilization and polarization. Our findings may provide insights into the pathogenic mechanism underlying the 1p34.2p34.3 deletion syndrome.

Keywords

MACF1; cortical progenitor; corpus callosum; heterotopia; autism-like behavior; progenitor proliferation

Introduction

Alterations in gene dosage due to the duplication or deletion of specific chromosome regions cause many neurodevelopmental disorders associated with autism spectrum disorders (ASD), intellectual disability (ID), and other related conditions (Lupski and Stankiewicz 2005; Geschwind 2011; Lee and Lupski 2006; Mefford et al. 2012). A microdeletion on chromosome 1p34.2p34.3 has been identified in multiple human patients, who, for the most part, exhibit ASD, ID, microcephaly, hypotonia, and facial dysmorphism (Vermeer et al. 2007; Kumar et al. 2010; Dagklis et al. 2016). Among the genes deleted in this chromosomal segment is *Microtubule Actin Crosslinking Factor 1* (*MACF1*).

MACF1 is a cytoskeletal linker protein that interacts with both F-actin and microtubules via an actin-binding domain near its N-terminus and a microtubule-binding domain near its C-terminus, respectively (Moffat et al. 2017). We previously showed that MACF1 regulates neuronal migration via microtubule dynamics and GSK-3 signaling in the developing brain (Ka et al. 2014b; Ka and Kim 2016). MACF1 is also required for neurite arborization and outgrowth, which are important for the establishment of neuronal connections in the brain (Ka and Kim 2016). These findings suggest a critical contribution of MACF1 to neuronal differentiation during later stages of brain development. However, little is known about the function of MACF1 and its associated mechanisms relating to neural progenitor regulation during the early stage of brain development.

The cerebral cortex is a central brain region, which controls complex neural behaviors (Geschwind and Rakic 2013). The size of the cerebral cortex depends on the balanced control of neural progenitor proliferation and maintenance during development (Chenn and Walsh 2002). Radial glial cells are the major progenitors in the developing cerebral cortex and their polarized fibers attached to the apical and basal surfaces of the cerebral cortex play a critical role in cell division (Gotz and Huttner 2005; Huttner and Kosodo 2005). While radial fibers span vertically along the entire cerebral cortex, their somas are strictly confined within the ventricular and subventricular zones. This distinct localization of radial soma is mediated by the actin and microtubule cytoskeleton and is essential for the precise control of neural progenitor proliferation (Messier and Auclair 1973; Gotz and Huttner 2005).

Here we investigate the function of MACF1 in neural progenitor proliferation during cortical development as well as in progenitors' apicobasal polarity. Conditional knockout strategies

were employed to target *Macf1* specifically in developing cortical progenitors in mice. We provide evidence that MACF1 maintains the cortical progenitor pool via regulation of radial fiber polarity during development. We also report that *Macf1* knockout mice demonstrate social and emotional behavior deficits. These findings support the proposition that loss of *MACF1* expression may be responsible for at least some of the anatomical and behavioral abnormalities produced by de novo microdeletion of chromosome 1p34.2p34.3.

Materials and Methods

Mice

Mice were handled in accordance with the animal protocol approved by the Institutional Animal Care and Use Committee (IACUC) at the University of Nebraska Medical Center and Kent State University (protocols #: 10–077-09, 464 WK 18–08). The *Macf1* floxed mouse was described previously (Wu et al. 2011). The Emx1-Cre mouse was purchased from The Jackson laboratory (Stock No: 005628). Embryonic age for mouse embryos was determined by checking breeder dams for vaginal plugs each morning. Embryonic days were then counted from that point (E0.5). All experimental procedures met National Institutes of Health guidelines for the care and use of laboratory animals.

Immunostaining

Immunostaining of brain sections or dissociated neural cells was performed as described previously (Kim et al. 2004; Ka et al. 2016b). The following primary antibodies were used: Mouse anti-NeuN (EMD Millipore, MAB337), rat anti-neural cell adhesion molecule L1 (EMD Millipore, MAB5272), rabbit anti-TBR1 (Abcam, ab31940), rabbit anti-CUX1 (Santa Cruz, sc-13024), chicken anti-MAP2 (Abcam, ab5392), rabbit anti-GFAP (Abcam, ab7260), rabbit anti-Ki67 (Cell Signaling, #9129), rabbit anti-phospho-Histone H3 (Cell Signaling, #9701S), mouse anti-BrdU (BD Biosciences, 555627), chicken anti-Tbr2 (EMD Millipore, ab15894), rabbit anti-BLBP (Abcam, ab32423), mouse anti-Nestin (PhosphoSolutions, 1435-NES), rabbit anti-ARL13B (Abcam, ab83879), rabbit anti-Acetyl-α-Tubulin (Cell Signaling, #5335), chicken anti-GFP (Thermo Fisher, A10262), rabbit anti-GFP (Thermo Fisher, A11122) and mouse anti-MACF1 (Santa Cruz, sc-377532). Alexa Fluor568-Phalloidin (Thermo Fisher, A12380) was used to stain polymerized actin. Appropriate secondary antibodies conjugated with Alexa Fluor dyes (Thermo Fisher) were used to detect primary antibodies. The purpose of using each antibody is listed in Table1.

In utero electroporation

In utero electroporation was performed as described previously (Ka and Kim 2018; Ka et al. 2016a). Briefly, timed pregnant female mice from E13.5 of gestation were deeply anesthetized, and the uterine horns were gently exposed by laparotomy. The lateral ventricles of an embryonic brain were injected with plasmid DNA (2 μg/μl) and 0.001% fast green (Sigma-Aldrich) using a Picospritzer II (Parker Hannifin). Electroporation was achieved by placing two sterile forceps-type electrodes on opposing sides of the uterine sac around the embryonic head and applying a series of short electrical pulses using a BTX ECM 830 electroporator (Harvard Apparatus) (five pulses with 100 ms length separated by 900 ms intervals were applied at 45 V).

Morphometry

Images of brain sections at periodic distances along the rostro-caudal axis were taken with the Zeiss LSM710 confocal microscope. Stereological analysis of immunostained cells was performed as described preciously (Kim et al. 2006; Dagklis et al. 2016). Cells in a field of 0.2 or 0.4 mm^2 within one-in-six series of 40 μm coronal sections throughout the rostro-caudal extent of the cerebral cortex. The images were subjected to software-driven particle analysis with automatic machine-set thresholding in ImageJ, thus eliminating subjective investigator bias. Then, a particle parameter enumeration analysis was followed for size exclusion at minimum of 10 $pixel^2$. The blue channel images were used to assess background cells. For analyzing cultured cells, more than 20 fields scanned horizontally and vertically were examined for each condition. Cell numbers were described in figure legends. The calculated values were averaged, and some results were recalculated as relative changes versus control.

BrdU administration and cell cycle analysis

BrdU injection and cell cycle analysis were performed as described previously (Kim et al. 2009; Ka et al. 2014a; Ka et al. 2017b). Intraperitoneal injection of BrdU (20mg per kg body weight) was performed into pregnant mice at E13.5–14.5. For the analysis of cell cycle re-entry, BrdU was administered to control and mutant mice for 24 h. The ratio of cells labeled with BrdU and Ki67 to total cells that incorporated BrdU was determined. For the analysis of cell cycle length, the ratio of progenitor cells positive for Ki67 and BrdU to the total Ki67 labeled cells was assessed after a 30 min BrdU pulse.

Behavioral assays

All behavioral assays were done during light cycle. Behavior recording and analysis were performed by a researcher blinded to the genotype of each mouse. Health conditions including weights, activity and feeding were checked prior to assays. Behavioral assays were performed as previously described (Jung et al. 2016; Jung et al. 2017; Smith et al. 2020).

Open field test: A mouse was placed near the wall-side of a 35 × 42 cm open-field arena, and the movement of the mouse was recorded by a camera for 5 min. The recorded video file was further analyzed using EthoVision XT 7.0 software (Noldus). Total distance moved and average velocity of movement were recorded. The number of entries into, and the overall time spent in, the center of the arena (15 × 15 cm imaginary square) were also measured. The open field arena was cleaned with 70% ethanol between each trial.

Novel object recognition test: Following habituation to an open field arena (35 × 42 cm) for 5 min, the test mouse was removed from the arena and two identical objects with size (10.5 × 4.5 × 2.5 cm) were placed in the opposite corners of the arena, 7 cm from the side walls. Then the test mouse was reintroduced into the center of the arena and allowed to explore the arena including the two novel objects for 10 min. After 6 h, one object was replaced with another novel object that was of similar size but different shape and color than the previous object. The same test mouse was placed in the arena to explore the two objects for 10 min.

Three-chamber test for social interaction and novelty behavior: A rectangular and transparent Plexiglas box divided by walls into three equal-sized compartments (Ugobasile) was used. For sociability testing, the test mouse was moved to the center chamber (chamber 2) with the entrances to the two connecting chambers blocked. A stimulus mouse (unfamiliar mouse) designated as “stranger 1” was placed in a wire enclosure in chamber 1. Then, the openings to the flanking two chambers (1 and 3) were opened and the test mouse was allowed to explore the entire apparatus for 10 min. For the social novelty test, the stranger 1 mouse was randomly placed in one of the enclosures in which the test mouse had the choice of whether to investigate the stranger 1 mouse or a novel mouse, designated “stranger 2”. This novel mouse was taken from a different home cage and placed into the remaining empty wire enclosure. Time spent sniffing each partner by the test mouse was recorded for 10 min in both sociability and social novelty behavior tests.

Rearing test: A test mouse was placed in a clean 300 ml glass beaker (Fisherbrand) and filmed for 5 minutes. The number of times reared and the total duration of rearing were recorded. A rearing even was only counted when both hindpaws were fully extended. The beaker was cleaned with 70% ethanol between each trail.

Grip strength test: A mouse was suspended upside-down from a wire mesh approximately 60 cm from a padded surface for a maximum of 2 minutes as described elsewhere (Deacon 2013). The mean latency to fall for each mouse was recorded in three trials with at least a 30 min break between trials. The wire mesh was cleaned with 70% ethanol between each trial.

Statistical analysis

Normal distribution was tested using the Kolmogorov–Smirnov test and variance was compared. Unless otherwise stated, statistical significance was determined by two-tailed unpaired Student’s t-test for two-population comparison and one-way or two-way ANOVA followed by Bonferroni correction test for multiple comparisons. Data were analyzed using GraphPad Prism and presented as mean (+/−) SEM. P values are indicated in figure legends. To determine and confirm sample sizes (*N*), we performed a power analysis. The values for the power (1-β) and the type I error rate (α) were 0.8 and 0.05 (or 0.01), respectively. Each experiment in this study was performed blind and randomized.

Results

Macf1 deletion in cortical progenitors leads to cortical malformations

To examine the roles of MACF1 in neural progenitor proliferation during cerebral cortical development, we crossed *Macf1* floxed mice with an Emx1-Cre mouse line that expresses Cre recombinase by embryonic day 9.5 (E9.5) in cortical neural progenitors (Gorski et al. 2002). *Macf1*$^{F/F}$*; Emx1-Cre* (*Macf1*-cKO) mice survived into adulthood, however, they exhibited a reduced survival rate compared to control (*Macf1*$^{F/W}$*; Emx1-Cre*) mice (Fig. 1a and 1b). *Macf1*-cKO mice also showed reduced body and brain weights at 8 weeks of age (Fig. 1c and 1d). Cortical area, A-P length and cortical length were similarly decreased in

Macf1-cKO brains compared to those in controls (Fig. 1e and 1f). It is noted that while the absolute weight and size of the *Macf1*-cKO brain were decreased, relative brain weight and size were elevated in *Macf1*-cKO mice compared to controls (Supplementary Figure 1).

Macf1-cKO brains exhibited thicker cerebral cortices than control brains, while they had smaller hippocampal areas (Fig. 2a and 2b). *Macf1*-cKO brains also displayed a pattern of subcortical band heterotopia (SBH) with aggregated NeuN or MAP2-positive neuronal masses throughout the cerebral cortex (Fig. 2c). GFAP-positive astrocytes were not generally found in the control cortex, but readily observed in the *Macf1*-cKO brain. Interestingly, *Macf1*-cKO brains had a double cortex phenotype featuring a second, ectopic layer of gray and white matter (Fig. 2d).

Disrupted cortical lamination in *Macf1*-cKO brains

Next, we sought to determine if the heterotopic or double cortex exists at early developing ages. Thus, we examined cerebral neuron positioning in control and *Macf1*-cKO mice at P3. In control brains, TBR1-positive deeper layer neurons were mostly restricted to layer VI, while they appeared to be evenly distributed throughout cortical layers of *Macf1*-cKO brains (Fig. 3a and 3b). Similar patterns were seen with upper layer CUX1-positive neurons. Control brains showed that CUX1-positive neurons were localized in cortical layers II-IV. However, *Macf1*-cKO brains exhibited abnormal dispersal of CUX1-positive neurons throughout the cortex. We also examined cortical layering within superficial layers I and II. Control brains displayed a clear separation between the pial surface and layer II (Fig. 3c). DAPI-positive, non-neuronal cells were densely concentrated in a straight line along the pial surface, while NeuN-negative Cajal–Retzius cells were localized in cortical layer I. NeuN-positive pyramidal neurons were populated in cortical layer II-III. In *Macf1*-cKO brains, however, the pial surface was not clearly defined and non-neuronal cells were interspersed within layer I, II, and III. Together, these results show that cortical progenitor-specific *Macf1* deletion causes abnormal neuronal placement, leading to pronounced malformations of the cerebral cortex.

Macf1 deletion alters cortical progenitor proliferation and the cell cycle

We investigated cortical progenitor proliferation in control and *Macf1*-cKO brains. Ki67 immunostaining labels actively proliferating cells. At E14.5, the number of Ki67-positive progenitors in *Macf1*-cKO brains was increased by 92%, compared to controls (Fig. 4a and 4b). Ki67-positive proliferating progenitors accumulated in the subventricular zone (SVZ) and ventricular zone (VZ) of control brains (Fig. 4a and 4c). This notable localization of progenitors was severely disrupted in *Macf1*-cKO brains. Instead, the proliferating progenitors were scattered throughout the cerebral cortex. We also assessed cells in the mitotic phase by immunostaining for phospho-histone H3. Similar to the Ki67 results, there was a 116% increase in the number of phospho-histone H3-positive mitotic cells in *Macf1*-cKO brains, compared to controls (Fig. 4d and 4e). Phospho-histone H3-positive mitotic cells in control brains were distinctively positioned within the VZ, but they appeared to be spread throughout all cortical layers in *Macf1*-cKO brains (Fig. 4d and 4f). Additionally, we assessed intermediate neural progenitors using TBR2 immunostaining. The number of TBR2-positive intermediate progenitors in *Macf1*-cKO cerebral cortices was 98% higher

than the number in controls (Fig. 4g and 4h). TBR2-positive intermediate progenitors strictly localized within the SVZ of control cortices, whereas they were spread out in *Macf1*-cKO cortices (Fig. 4g and 4i). These results demonstrate that MACF1 is essential for normal proliferation and region-specific confinement of cortical neural progenitors during development.

To identify the underlying cause of the increase in progenitor proliferation in the *Macf1*-cKO cerebral cortex, we examined cell cycle speed because cell cycle dysregulation could lead to the observed proliferation change. Cell cycle progression is a key control mechanism that accounts for neuron numbers in the developing brain (Dehay and Kennedy 2007). Cell-cycle re-entry/exit is an indication of cell cycle progression (Chenn and Walsh 2002). Cell cycle speed was assessed by the number of Ki67/BrdU double-positive cells divided by the total Ki67-positive cells after a 30 minute BrdU pulse as described in previous studies (Kim et al. 2009; Ka et al. 2014a; Ka et al. 2017b). In essence, the ratio of Ki67/BrdU double-positive cells to the total Ki67-expressing population estimates the proportion of cells that are both actively proliferating and entered the S-phase of the cell cycle in that 30-minute timespan (Kee et al. 2002). Cell cycle speed was increased by 60% in *Macf1*-cKO cerebral cortices compared to controls (Fig. 5a and 5b). We also measured cell cycle re-entry in *Macf1*-cKO progenitors by counting the number of Ki67/BrdU double-positive cells divided by the total number of BrdU-positive cells after a 24 h BrdU pulse. In this experiment, Ki67/BrdU double positive neurons represent cells that were born during the 24 h pulse and are still actively proliferating, whereas cells that are only BrdU-positive were born during the 24 h pulse and have exited the cell cycle (Kee et al. 2002; Ka et al. 2014a). The number of progenitors re-entering the cell cycle was 46% higher in *Macf1*-cKO cerebral cortices than in controls (Fig. 5c and 5d). Our data suggest that increased speed of, and re-entry into, the progenitor cell cycle may contribute to the double cortex phenotype as well as SBH in the *Macf1*-cKO brain.

Abnormal radial glial polarity and integrity in *Macf1*-cKO brains

In order to understand the abnormal positioning of proliferating progenitors in *Macf1*-cKO mice, we first examined the role of MACF1 in radial glial development. We immunostained the E14.5 cerebral cortex with an antibody to BLBP, a marker for radial glial neural progenitors. Radial progenitors extend apical radial fibers toward the VZ and basal fibers toward the marginal zone of the cerebral cortex. In control brains, BLBP-positive radial glial progenitors developed straight, linear basal fibers attached to the pial surface (Fig. 6a). Radial glial progenitors in *Macf1*-cKO brains, on the other hand, showed no clear basal fibers toward the pia. The intensity of BLBP staining on *Macf1*-cKO pial surfaces was 38% lower, when compared to controls (Fig. 6b). Moreover, it appeared that BLBP-positive radial glial fibers in the VZ of control brains filled the VZ, while the fibers were more sparse in the *Macf1*-cKO VZ (Fig. 6c). We further assessed the apical and basal radial fibers attached to the VZ and pial surface, respectively, by labelling radial glial progenitors at low density using *in utero* electroporation of a BLBP-EGFP construct. In control brains, EGFP-labeled apical radial fibers attached to the VZ surface (Fig. 6d and 6e). In contrast, *Macf1*-cKO radial progenitors did not appear to develop nor attach as many apical fibers as control progenitors. Similarly, basal fibers of control radial progenitors robustly anchored to the pial

surface of the cerebral cortex. However, there was a marked reduction in pial attachment of basal fibers in *Macf1*-cKO radial progenitors. These results suggest a critical role of MACF1 in the establishment and maintenance of radial progenitor polarity.

Next, we assessed cytoskeletal dynamics and stability of radial progenitors in the *Macf1*-cKO VZ. MACF1 was broadly expressed in the developing cerebral cortex and accumulated in the VZ and upper cortical areas near the MZ where Nestin-positive radial progenitor somas and fiber terminals are located, respectively (Fig. 7a). Phalloidin staining of cortical sections showed that polymerized actin was preferentially located within the apical ventricular zone in the control brain (Fig. 7b). However, phalloidin-stained, polymerized actin was broadly present throughout the cerebral cortex in *Macf1*-cKO mice. Primary cilia, which are microtubule-based cytoskeleton structures necessary for neuronal migration, were also assessed by immunostaining for the cilia marker ARL13B. Expression of ARL13B appeared to be randomly dispersed in the *Macf1*-cKO cortex while its expression was restricted to the surface of the VZ in the control (Fig. 7b and 7c). Microtubule stability was further examined in the *Macf1* mutant cortex. Stabilized microtubules marked by acetylated-tubulin were localized along the VZ surface within Nestin-positive radial progenitors in the control cortex (Fig. 7d and 7e). In contrast, acetylated-tubulin staining was spread throughout the *Macf1*-cKO cerebral cortex. Together, these results suggest that MACF1 plays an important role in establishing and/or maintaining cytoskeletal integrity and polarity in radial progenitors during cortical development.

Finally, we examined the corpus callosum in the *Macf1*-cKO brain because corpus callosum abnormalities are associated with neurodevelopmental disorders (Kappeler et al. 2007; Raybaud 2010). Nissel staining showed that callosal axons were clearly bundled and crossed the midline at the corpus callosum along the rostro-caudal axis in the control brain (Supplementary Fig. 2). However, callosal axons in the *Macf1*-cKO brain exhibited a thinner bundle at the rostral area and failed to cross the midline caudally.

Behavioral outcomes of cortical *Macf1* deletion

Compared to controls, *Macf1*-cKO mice showed no significant change in locomotion as the total distance moved and mean travel velocity in the open field test were not significantly changed. There were also no differences in basic motor functions including rearing frequency and grip strength (Fig. 8a and 8b). *Macf1*-cKO mice demonstrated unusual exploratory behavior in the open field, however, spending significantly less time in the center of the field and making fewer overall enter entries (Fig. 8c and 8d). This phenotype of center avoidance is generally indicative of anxiety-like behavior. In the three-chamber social interaction assay, we observed no significant difference between *Macf1*-cKO mice and controls in the sociability portion of the test. Mice from each genotype spent significantly more time in a chamber containing an unfamiliar, wild-type mouse than in an empty chamber. In the social novelty portion of the test, however, control mice spent significantly more time in the chamber containing a novel peer than a more familiar mouse, while *Macf1*-cKO mice did not show a significant preference for either chamber (Fig. 8e). This indicates that conditional deletion of *Macf1* may lead to social anxiety in mice. To exclude recognition memory deficits as an explanation for this aberrant social novelty

behavior, we performed a novel object recognition test. *Macf1*-cKO mice and control mice both spent significantly more time exploring a novel object, rather than a familiar one (Fig. 8f). Altogether, *Macf1*-cKO mice exhibit baseline anxiety-like behavior and social anxiety.

Discussion

In this study, we have defined a critical role for MACF1 in cortical neural progenitors during development. A schematic model of radial progenitor polarity and neuronal placement within the cerebral cortex in the absence or presence of MACF1 is presented in Figure 9. Deletion of *Macf1* in cortical neural progenitors leads to abnormal neuronal positioning and corresponding malformations of the cerebral cortex via disruption of radial progenitor polarity. Elevated expression of MACF1 at the VZ surface, the main proliferative zone during cortical development, suggests its role in cortical progenitor regulation. Indeed, we demonstrate here that MACF1 is crucial for neural progenitor localization and proliferation. Conditional deletion of *Macf1* in mice using an Emx1-Cre driver disrupts radial progenitor homeostasis, resulting in abnormal neuronal positioning and an increase in the number of proliferating cells in the developing brain. This is similar to what is seen with deletion of 14–3-3, a protein that interacts with MACF1. Knockout of 14–3-3 also leads to an aberrant distribution of progenitor cells in the developing cerebral cortex along with an overall increase in their number (Toyo-oka et al. 2014). The increased number of progenitors does not result in a larger brain in the *Macf1-cKO* mouse. However, the relative brain size after normalization by a whole body weight is increased, confirming the promoting effect of *Macf1* deletion in progenitor proliferation.

Macf1 is not the only gene contained in this region of chromosome 1. Notable other genes found within the interstitial microdeletion reported by Dagklis et al. (Dagklis et al. 2016), for example, include *GLUT1*, which has been linked to hyperactivity and developmental delay (Vermeer et al. 2007; Aktas et al. 2010), the autism candidate gene *RIMS3* ((Kumar et al. 2010), *GRIK3*, which is associated with developmental delay (Takenouchi et al. 2014), and AGO1/AGO3, which are linked with neurocognitive deficits (Tokita et al. 2015). Nearby microdeletions, such as a 1p34.3p34.2 deletion reported in 2018 (Jacher and Innis 2018), also impact neurodevelopment and do not always include *MACF1.* While the current study indicates that *Macf1* deletion in mice may be sufficient to cause several of the phenotypes seen in human patients, there is likely a summative effect, in which the downstream effects of losing several genes combine to influence brain development.

Here we show that *Macf1* deletion causes major defects in radial progenitor polarity. Our results suggest that depletion of MACF1 during early corticogenesis interferes with F-actin formation and destabilizes microtubules at the VZ surface. Thus, radial glial apical and basal fibers are prevented from anchoring and maintaining in the VZ and Pia surface, respectively. This matches up well with what occurs with loss of MACF1 during retinal development, namely the abolishment of ciliogenesis and disruption of apicobasal polarity (May-Simera et al. 2016). Similarly, MACF1 is an important regulator of apicobasal polarity in mammalian intestinal cells in which radial centrosome-centered microtubule organization inhibits epithelial polarity (Noordstra et al. 2016). This is further consistent with the requirement of stabilized (acetylated) tubulin for proper neurite formation in

cortical neurons (Ka et al. 2014b; Ka et al. 2017a). The destabilization of microtubules during early corticogenesis (E9-E14.5) and disruption of neuronal migration and neurite outgrowth during later stages of brain development (E14.5-P0) (Ka et al. 2014b) likely both contribute to the behavioral phenotypes we report here, though we did not examine neurite growth dynamics at later stages in the current study.

SBH, also known as subcortical laminar heterotopia or double cortex syndrome, is a cortical malformation characterized by the presence of bilateral bands of heterotopic grey matter that results from the aberrant migration of neurons during cortical development (Dobyns et al. 1996; Pang et al. 2008). Conditional deletion of *Macf1* in mice using an Nex-Cre driver disrupts neuron homeostasis, resulting in abnormal neuronal positioning, but did not show radial glial defects in the developing brain (Ka et al. 2014b). This is likely due to Nex-Cre expression being largely restricted to pyramidal neurons starting at E11.5 and absent from proliferating neural progenitors in the VZ (Goebbels et al. 2006). Our data demonstrate that MACF1 is critical in restricting radial progenitors within the ventricular zone. This spatial arrangement of radial progenitors appears to rely on the MACF1's role in anchoring apical and basal radial fibers of these progenitors to the VZ and pial surface, respectively. The failure of this confinement leads to radial progenitors ectopically. This abnormal positioning of radial progenitors, caused by disconnection to the VZ, likely disrupts apical inputs that are required to maintain cell cycle speed and re-entry, leading to excessive proliferation in the *Macf1*-deleted brain. This cellular mechanism may explain the primary origin of heterotopia in the absence of MACF1. Classical forms of SBH have been primarily linked to abnormal neuronal migration. Our results suggest that destabilization of actin and microtubule cytoskeletons at the VZ and pia alters radial glial polarity leading to ectopic proliferative zones of cortical progenitors. Thus, defective polarity and proliferation of radial progenitors, rather than strictly neuronal migration deficits, may explain some cases of SBH. Our study provides with new insights for SBH pathology by demonstrating the MACF1 function in cortical progenitor regulation. The abnormal apical detachment due to MACF1 dysfunction may broadly influence other neurodevelopmental disorders related to developing progenitor problems. It remains to be seen if this phenomenon is common in other developmental disorders related to SBH. Further research will be required to determine exactly which downstream pathways and/or mechanisms influenced by MACF1 contribute to this phenotype.

The corpus callosum is one of the largest white matter tracts in the human brain, serving to physically and functionally connect the hemispheres of the cerebral cortex and plays critical roles in brain functions (Tomasch 1954). In humans, 3–5% of patients with neurodevelopmental disorders present with partial or complete agenesis of the corpus callosum (Jeret et al. 1985; Bodensteiner et al. 1994). Agenesis of the corpus callosum is also associated with 70% cases of SBH (Barkovich et al. 2005). We find that elimination of MACF1 results in corpus callosum defects. It will be interesting to examine if the 1p34.2p34.3 microdeletion syndrome involves corpus callosum agenesis.

Overall locomotion and limb strength are not significantly affected, but in the open field test *Macf1*-cKO mice spend the vast majority of their time exploring the periphery, rarely venturing into the center of the field. This thigmotaxic behavioral pattern has classically

been linked to heightened anxiety (Crawley 1999; Bailey and Crawley 2009; Belzung 2001). Despite extensive cortical and hippocampal abnormalities, *Macf1*-cKO mice display no significant deficits in non-spatial memory, as measured using the novel object recognition task. In the three-chamber social test, *Macf1*-mice show defective social novelty behavior, indicative of social anxiety-like behavior, but no overall deficit in general sociability. It may not be surprising that the behavioral effects of *Macf1* deletion in the developing cortex is not sufficient to mirror all of the behavioral defects seen in human patients. Indeed, the majority of emotional and social behaviors are more strongly linked to deficits in inhibitory interneurons, often in brain regions outside the cerebral cortex, not in the excitatory cortical neurons in our conditional deletion (Dulawa et al. 2004; Gorski et al. 2002; Iwasato et al. 2004). However, it is clear that conditional deletion of *Macf1* in radial progenitor cells and their progeny leads to marked behavioral abnormalities and it is reasonable to assume that global deletion of *Macf1* may result in more diverse phenotypes.

Supplementary Material

Refer to Web version on PubMed Central for supplementary material.

Funding

Research reported in this publication was supported by an award from the National Institute of Neurological Disorders and Stroke of the National Institutes of Health under award number R01NS091220 to WYK and a grant from the National Research Foundation of Korea under grant number NRF-2019R1A2C1009006 to MK.

Reference

Aktas D, Utine EG, Mrasek K, Weise A, von Eggeling F, Yalaz K, Posorski N, Akarsu N, Alikasifoglu M, Liehr T, Tuncbilek E (2010) Derivative chromosome 1 and GLUT1 deficiency syndrome in a sibling pair. Mol Cytogenet 3 (1):10. doi:10.1186/1755-8166-3-10 [PubMed: 20509907]

Bailey KR, Crawley JN (2009) Anxiety-Related Behaviors in Mice. In: nd, Buccafusco JJ (eds) Methods of Behavior Analysis in Neuroscience. Frontiers in Neuroscience. Boca Raton (FL),

Barkovich AJ, Kuzniecky RI, Jackson GD, Guerrini R, Dobyns WB (2005) A developmental and genetic classification for malformations of cortical development. Neurology 65 (12):1873–1887. doi:10.1212/01.wnl.0000183747.05269.2d [PubMed: 16192428]

Belzung C (2001) Rodent models of anxiety-like behaviors: are they predictive for compounds acting via non-benzodiazepine mechanisms? Curr Opin Investig Drugs 2 (8):1108–1111

Bodensteiner J, Schaefer GB, Breeding L, Cowan L (1994) Hypoplasia of the corpus callosum: a study of 445 consecutive MRI scans. J Child Neurol 9 (1):47–49. doi:10.1177/088307389400900111 [PubMed: 8151082]

Chenn A, Walsh CA (2002) Regulation of cerebral cortical size by control of cell cycle exit in neural precursors. Science 297 (5580):365–369. doi:10.1126/science.1074192 [PubMed: 12130776]

Crawley JN (1999) Behavioral phenotyping of transgenic and knockout mice: experimental design and evaluation of general health, sensory functions, motor abilities, and specific behavioral tests. Brain Res 835 (1):18–26. doi:10.1016/s0006-8993(98)01258-x [PubMed: 10448192]

Dagklis T, Papageorgiou E, Siomou E, Paspaliaris V, Zerva C, Chatzis P, Thomaidis L, Manolakos E, Papoulidis I (2016) Prenatal diagnosis of 1p34.3 interstitial microdeletion by aCGH in a fetus with jaw bone abnormalities. Mol Cytogenet 9:77. doi:10.1186/s13039-016-0288-y [PubMed: 27713767]

Deacon RM (2013) Measuring the strength of mice. J Vis Exp (76). doi:10.3791/2610

Dehay C, Kennedy H (2007) Cell-cycle control and cortical development. Nat Rev Neurosci 8 (6):438–450. doi:10.1038/nrn2097 [PubMed: 17514197]

Dobyns WB, Andermann E, Andermann F, Czapansky-Beilman D, Dubeau F, Dulac O, Guerrini R, Hirsch B, Ledbetter DH, Lee NS, Motte J, Pinard JM, Radtke RA, Ross ME, Tampieri D, Walsh CA, Truwit CL (1996) X-linked malformations of neuronal migration. Neurology 47 (2):331–339 [PubMed: 8757001]

Dulawa SC, Holick KA, Gundersen B, Hen R (2004) Effects of chronic fluoxetine in animal models of anxiety and depression. Neuropsychopharmacology : official publication of the American College of Neuropsychopharmacology 29 (7):1321–1330. doi:10.1038/sj.npp.1300433 [PubMed: 15085085]

Geschwind DH (2011) Genetics of autism spectrum disorders. Trends Cogn Sci 15 (9):409–416. doi:10.1016/j.tics.2011.07.003 [PubMed: 21855394]

Geschwind DH, Rakic P (2013) Cortical evolution: judge the brain by its cover. Neuron 80 (3):633–647. doi:10.1016/j.neuron.2013.10.045 [PubMed: 24183016]

Goebbels S, Bormuth I, Bode U, Hermanson O, Schwab MH, Nave KA (2006) Genetic targeting of principal neurons in neocortex and hippocampus of NEX-Cre mice. Genesis 44 (12):611–621. doi:10.1002/dvg.20256 [PubMed: 17146780]

Gorski JA, Talley T, Qiu M, Puelles L, Rubenstein JL, Jones KR (2002) Cortical excitatory neurons and glia, but not GABAergic neurons, are produced in the Emx1-expressing lineage. J Neurosci 22 (15):6309–6314. doi:20026564 [PubMed: 12151506]

Gotz M, Huttner WB (2005) The cell biology of neurogenesis. Nat Rev Mol Cell Biol 6 (10):777–788. doi:10.1038/nrm1739 [PubMed: 16314867]

Huttner WB, Kosodo Y (2005) Symmetric versus asymmetric cell division during neurogenesis in the developing vertebrate central nervous system. Curr Opin Cell Biol 17 (6):648–657. doi:10.1016/j.ceb.2005.10.005 [PubMed: 16243506]

Iwasato T, Nomura R, Ando R, Ikeda T, Tanaka M, Itohara S (2004) Dorsal telencephalon-specific expression of Cre recombinase in PAC transgenic mice. Genesis 38 (3):130–138. doi:10.1002/gene.20009 [PubMed: 15048810]

Jacher JE, Innis JW (2018) Interstitial microdeletion of the 1p34.3p34.2 region. Mol Genet Genomic Med. doi:10.1002/mgg3.409

Jeret JS, Serur D, Wisniewski K, Fisch C (1985) Frequency of agenesis of the corpus callosum in the developmentally disabled population as determined by computerized tomography. Pediatr Neurosci 12 (2):101–103 [PubMed: 2428024]

Jung EM, Ka M, Kim WY (2016) Loss of GSK-3 Causes Abnormal Astrogenesis and Behavior in Mice. Mol Neurobiol 53 (6):3954–3966. doi:10.1007/s12035-015-9326-8 [PubMed: 26179612]

Jung EM, Moffat JJ, Liu J, Dravid SM, Gurumurthy CB, Kim WY (2017) Arid1b haploinsufficiency disrupts cortical interneuron development and mouse behavior. Nat Neurosci 20 (12):1694–1707. doi:10.1038/s41593-017-0013-0 [PubMed: 29184203]

Ka M, Chopra DA, Dravid SM, Kim WY (2016a) Essential Roles for ARID1B in Dendritic Arborization and Spine Morphology of Developing Pyramidal Neurons. J Neurosci 36 (9):2723–2742. doi:10.1523/JNEUROSCI.2321-15.2016 [PubMed: 26937011]

Ka M, Condorelli G, Woodgett JR, Kim WY (2014a) mTOR regulates brain morphogenesis by mediating GSK3 signaling. Development 141 (21):4076–4086. doi:10.1242/dev.108282 [PubMed: 25273085]

Ka M, Jung EM, Mueller U, Kim WY (2014b) MACF1 regulates the migration of pyramidal neurons via microtubule dynamics and GSK-3 signaling. Dev Biol 395 (1):4–18. doi:10.1016/j.ydbio.2014.09.009 [PubMed: 25224226]

Ka M, Kim WY (2016) Microtubule-Actin Crosslinking Factor 1 Is Required for Dendritic Arborization and Axon Outgrowth in the Developing Brain. Mol Neurobiol 53 (9):6018–6032. doi:10.1007/s12035-015-9508-4 [PubMed: 26526844]

Ka M, Kim WY (2018) ANKRD11 associated with intellectual disability and autism regulates dendrite differentiation via the BDNF/TrkB signaling pathway. Neurobiol Dis 111:138–152. doi:10.1016/j.nbd.2017.12.008 [PubMed: 29274743]

Ka M, Kook YH, Liao K, Buch S, Kim WY (2016b) Transactivation of TrkB by Sigma-1 receptor mediates cocaine-induced changes in dendritic spine density and morphology in hippocampal and cortical neurons. Cell Death Dis 7 (10):e2414. doi:10.1038/cddis.2016.319 [PubMed: 27735948]

Ka M, Moffat JJ, Kim WY (2017a) MACF1 Controls Migration and Positioning of Cortical GABAergic Interneurons in Mice. Cereb Cortex 27 (12):5525–5538. doi:10.1093/cercor/bhw319 [PubMed: 27756764]

Ka M, Smith AL, Kim WY (2017b) MTOR controls genesis and autophagy of GABAergic interneurons during brain development. Autophagy 13 (8):1348–1363. doi:10.1080/15548627.2017.1327927 [PubMed: 28598226]

Kappeler C, Dhenain M, Phan Dinh Tuy F, Saillour Y, Marty S, Fallet-Bianco C, Souville I, Souil E, Pinard JM, Meyer G, Encha-Razavi F, Volk A, Beldjord C, Chelly J, Francis F (2007) Magnetic resonance imaging and histological studies of corpus callosal and hippocampal abnormalities linked to doublecortin deficiency. J Comp Neurol 500 (2):239–254. doi:10.1002/cne.21170 [PubMed: 17111359]

Kee N, Sivalingam S, Boonstra R, Wojtowicz JM (2002) The utility of Ki-67 and BrdU as proliferative markers of adult neurogenesis. J Neurosci Methods 115 (1):97–105. doi:10.1016/s0165-0270(02)00007-9 [PubMed: 11897369]

Kim WY, Horbinski C, Sigurdson W, Higgins D (2004) Proteasome inhibitors suppress formation of polyglutamine-induced nuclear inclusions in cultured postmitotic neurons. J Neurochem 91 (5):1044–1056. doi:10.1111/j.1471-4159.2004.02788.x [PubMed: 15569248]

Kim WY, Wang X, Wu Y, Doble BW, Patel S, Woodgett JR, Snider WD (2009) GSK-3 is a master regulator of neural progenitor homeostasis. Nat Neurosci 12 (11):1390–1397. doi:10.1038/nn.2408 [PubMed: 19801986]

Kim WY, Zhou FQ, Zhou J, Yokota Y, Wang YM, Yoshimura T, Kaibuchi K, Woodgett JR, Anton ES, Snider WD (2006) Essential roles for GSK-3s and GSK-3-primed substrates in neurotrophin-induced and hippocampal axon growth. Neuron 52 (6):981–996. doi:10.1016/j.neuron.2006.10.031 [PubMed: 17178402]

Kumar RA, Sudi J, Babatz TD, Brune CW, Oswald D, Yen M, Nowak NJ, Cook EH, Christian SL, Dobyns WB (2010) A de novo 1p34.2 microdeletion identifies the synaptic vesicle gene RIMS3 as a novel candidate for autism. J Med Genet 47 (2):81–90. doi:10.1136/jmg.2008.065821 [PubMed: 19546099]

Lee JA, Lupski JR (2006) Genomic rearrangements and gene copy-number alterations as a cause of nervous system disorders. Neuron 52 (1):103–121. doi:10.1016/j.neuron.2006.09.027 [PubMed: 17015230]

Lupski JR, Stankiewicz P (2005) Genomic disorders: molecular mechanisms for rearrangements and conveyed phenotypes. PLoS Genet 1 (6):e49. doi:10.1371/journal.pgen.0010049 [PubMed: 16444292]

May-Simera HL, Gumerson JD, Gao C, Campos M, Cologna SM, Beyer T, Boldt K, Kaya KD, Patel N, Kretschmer F, Kelley MW, Petralia RS, Davey MG, Li T (2016) Loss of MACF1 Abolishes Ciliogenesis and Disrupts Apicobasal Polarity Establishment in the Retina. Cell Rep 17 (5):1399–1413. doi:10.1016/j.celrep.2016.09.089 [PubMed: 27783952]

Mefford HC, Batshaw ML, Hoffman EP (2012) Genomics, intellectual disability, and autism. N Engl J Med 366 (8):733–743. doi:10.1056/NEJMra1114194 [PubMed: 22356326]

Messier PE, Auclair C (1973) Inhibition of nuclear migration in the absence of microtubules in the chick embryo. J Embryol Exp Morphol 30 (3):661–671 [PubMed: 4772391]

Moffat JJ, Ka M, Jung EM, Smith AL, Kim WY (2017) The role of MACF1 in nervous system development and maintenance. Semin Cell Dev Biol. doi:10.1016/j.semcdb.2017.05.020

Noordstra I, Liu Q, Nijenhuis W, Hua S, Jiang K, Baars M, Remmelzwaal S, Martin M, Kapitein LC, Akhmanova A (2016) Control of apico-basal epithelial polarity by the microtubule minus-end-binding protein CAMSAP3 and spectraplakin ACF7. J Cell Sci 129 (22):4278–4288. doi:10.1242/jcs.194878 [PubMed: 27802168]

Pang T, Atefy R, Sheen V (2008) Malformations of cortical development. Neurologist 14 (3):181–191. doi:10.1097/NRL.0b013e31816606b9 [PubMed: 18469675]

Raybaud C (2010) The corpus callosum, the other great forebrain commissures, and the septum pellucidum: anatomy, development, and malformation. Neuroradiology 52 (6):447–477. doi:10.1007/s00234-010-0696-3 [PubMed: 20422408]

Smith AL, Jung EM, Jeon BT, Kim WY (2020) Arid1b haploinsufficiency in parvalbumin- or somatostatin-expressing interneurons leads to distinct ASD-like and ID-like behavior. Scientific reports 10 (1):7834. doi:10.1038/s41598-020-64066-5 [PubMed: 32398858]

Takenouchi T, Hashida N, Torii C, Kosaki R, Takahashi T, Kosaki K (2014) 1p34.3 deletion involving GRIK3: Further clinical implication of GRIK family glutamate receptors in the pathogenesis of developmental delay. Am J Med Genet A 164A (2):456–460. doi:10.1002/ajmg.a.36240 [PubMed: 24449200]

Tokita MJ, Chow PM, Mirzaa G, Dikow N, Maas B, Isidor B, Le Caignec C, Penney LS, Mazzotta G, Bernardini L, Filippi T, Battaglia A, Donti E, Earl D, Prontera P (2015) Five children with deletions of 1p34.3 encompassing AGO1 and AGO3. Eur J Hum Genet 23 (6):761–765. doi:10.1038/ejhg.2014.202 [PubMed: 25271087]

Tomasch J (1954) Size, distribution, and number of fibres in the human corpus callosum. Anat Rec 119 (1):119–135 [PubMed: 13181005]

Toyo-oka K, Wachi T, Hunt RF, Baraban SC, Taya S, Ramshaw H, Kaibuchi K, Schwarz QP, Lopez AF, Wynshaw-Boris A (2014) 14–3-3epsilon and zeta regulate neurogenesis and differentiation of neuronal progenitor cells in the developing brain. J Neurosci 34 (36):12168–12181. doi:10.1523/JNEUROSCI.2513-13.2014 [PubMed: 25186760]

Vermeer S, Koolen DA, Visser G, Brackel HJ, van der Burgt I, de Leeuw N, Willemsen MA, Sistermans EA, Pfundt R, de Vries BB (2007) A novel microdeletion in 1(p34.2p34.3), involving the SLC2A1 (GLUT1) gene, and severe delayed development. Dev Med Child Neurol 49 (5):380–384. doi:10.1111/j.1469-8749.2007.00380.x [PubMed: 17489814]

Wu X, Shen QT, Oristian DS, Lu CP, Zheng Q, Wang HW, Fuchs E (2011) Skin stem cells orchestrate directional migration by regulating microtubule-ACF7 connections through GSK3beta. Cell 144 (3):341–352. doi:10.1016/j.cell.2010.12.033 [PubMed: 21295697]

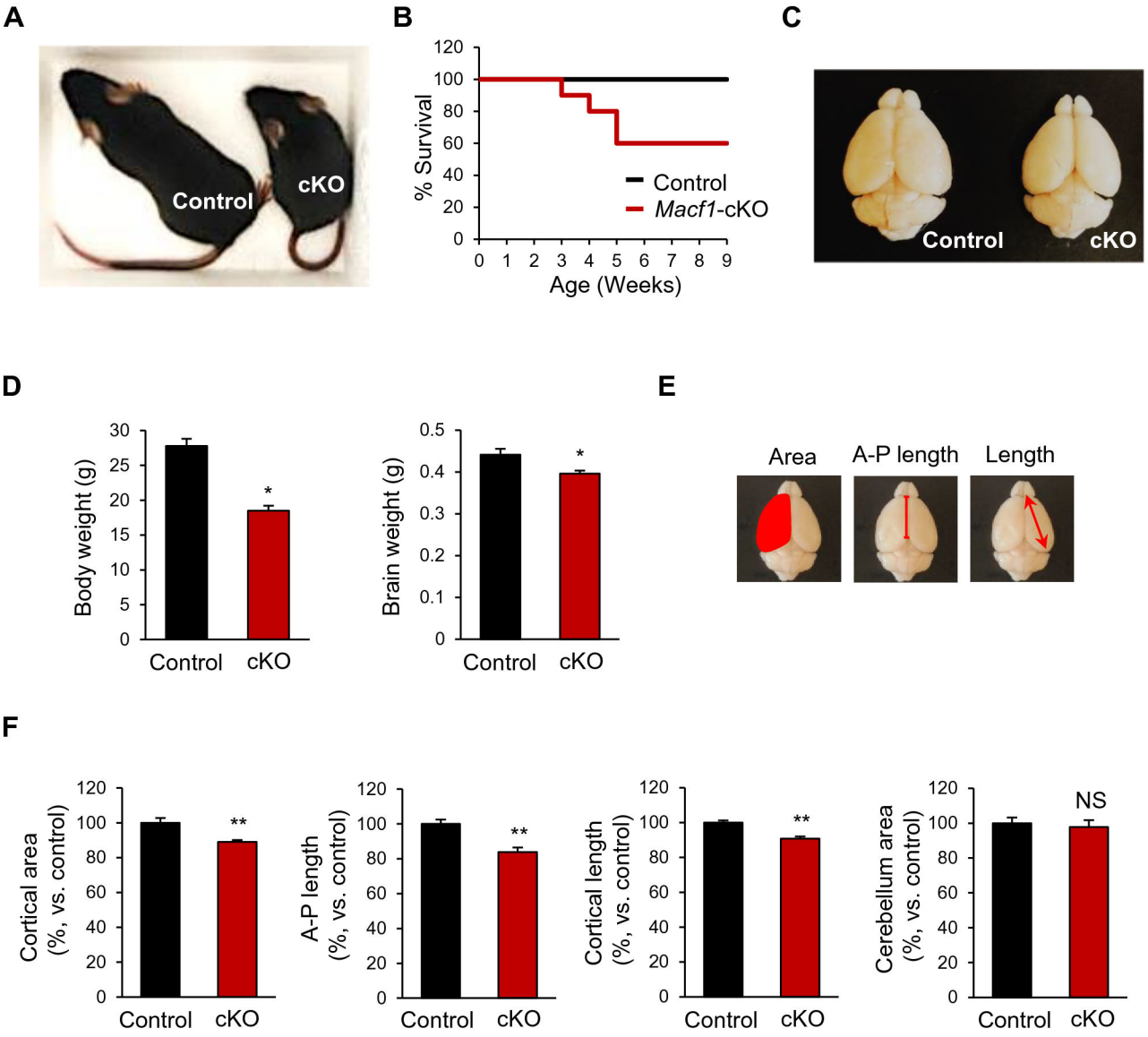

Fig. 1. Reduced brain size in *Macf1*-cKO mice

(**A**) Representative images of control (left) and *Macf1*-cKO (right) mice at the age of 2 months. (**B**) The survival curve of *Macf1*-cKO and control mice after the Kaplan-Meier method. N= 20 mice for littermate controls and 10 for *Macf1*-cKO mice. (**C**) Representative images of whole brains at age 2 months. (**D**) Quantifications of the body and brain weight of control and *Macf1*-cKO mice. N=5 mice for each condition. Statistical significance was determined by two-tailed Student's t-test. Data shown are the mean ± SEM. *$p < 0.05$. (**E and F**) Measurements of cortical parameters including the cortical area, anteroposterior (A-P) length, cortical length and cerebellum area. N= 5 mice for each condition. Statistical significance was determined by two-tailed Student's t-test. Data are shown as relative changes versus controls. **$p < 0.01$. NS: no significance.

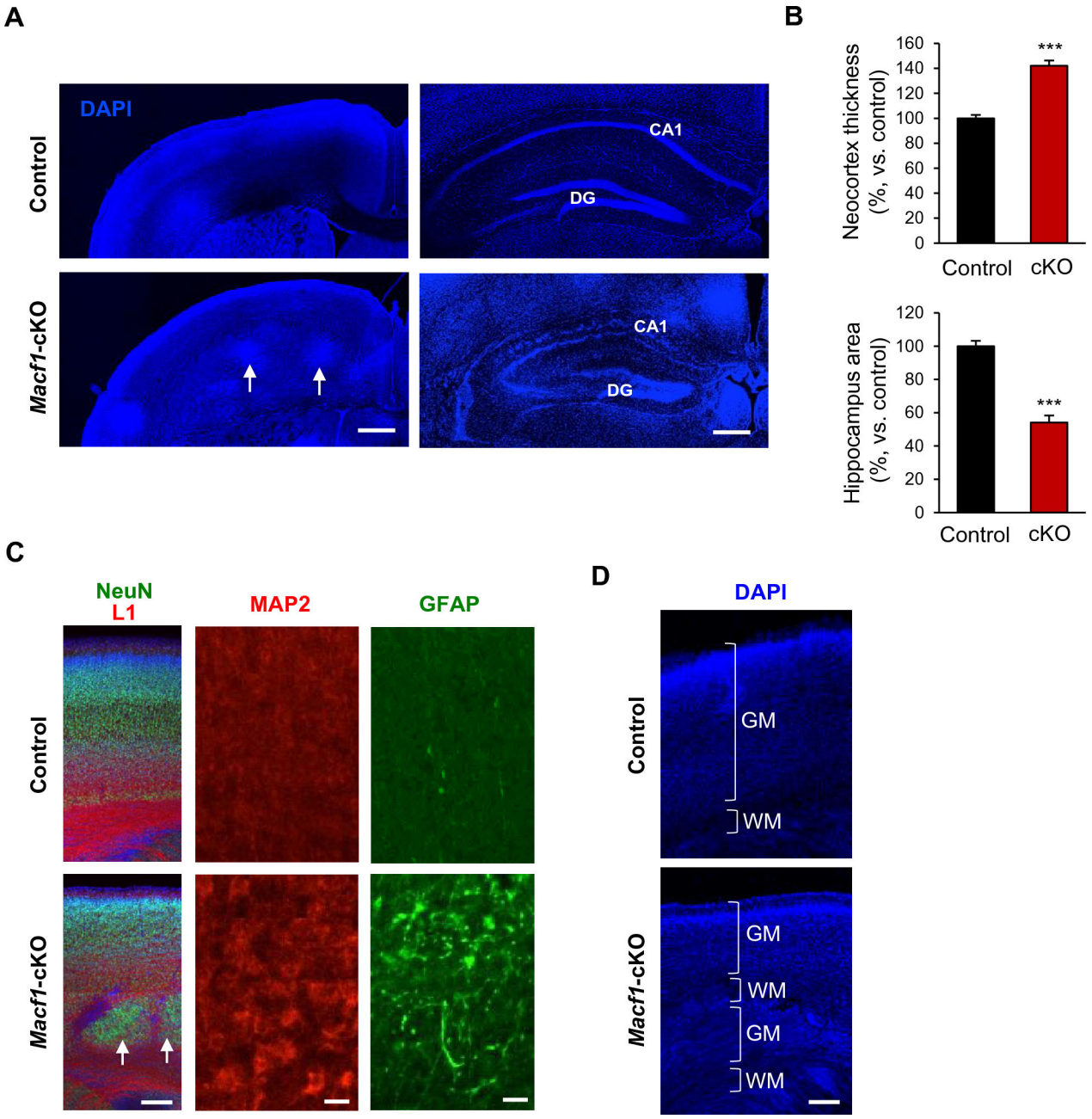

Fig. 2. Cortical malformation in *Macf1*-cKO mice

(**A**) Brain sections from 2-month-old control and *Macf1*-cKO mice were stained with DAPI. Arrows indicate SBH. Left and right panels show cerebral cortices and hippocampi, respectively. DG: dentate gyrus. Scale bars: 500 μm (left), 200 μm (right). (**B**) Quantifications of the cortical thickness and the hippocampal area of control and *Macf1*-cKO mice. N= 5 mice for each condition. Statistical significance was determined by two-tailed Student's t-test. Data are shown as relative changes versus controls. ***$p < 0.001$. (**C**) Immunostaining of cerebral cortices to L1, MAP2 and GFAP. Arrows indicate SBH. Scale bars: 200 μm (left), 20 μm (middle and right). (**D**) DAPI-stained cerebral cortices. GM: gray matter; WM: white matter. Scale bars: 200 μm.

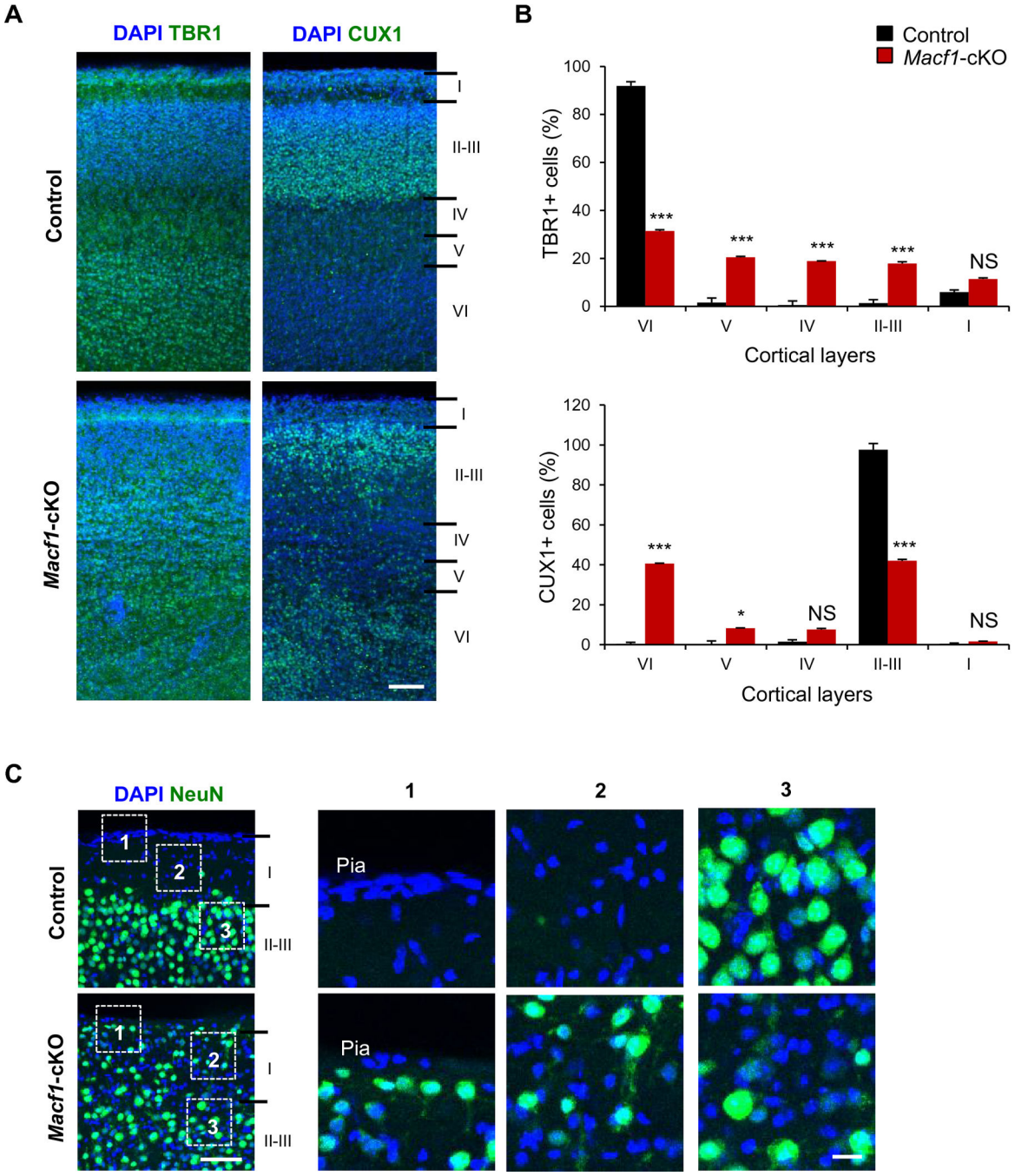

Fig. 3. Abnormal neuronal positioning in *Macf1*-cKO brains

(**A**) Cerebral cortices from P3 control and *Macf1*-cKO mice were immunostained with an anti-TBR1 or anti-CUX1 antibody. Scale bars: 100μm. (**B**) Localization of TBR1-positive or CUX1-positive neurons was quantified in control and *Macf1*-cKO cortices. N= 5 mice for each condition. Statistical significance was determined by two-way ANOVA with Bonferonni correction test. *$p < 0.05$, ***$p < 0.001$ vs. control. (**C**) NeuN immunostaining of cortical sections of control and *Macf1*-cKO brains. Right panels are higher magnification

images of the dotted boxes in the left panels. Scale bars: 50 μm (left panels), 10 μm (right panels).

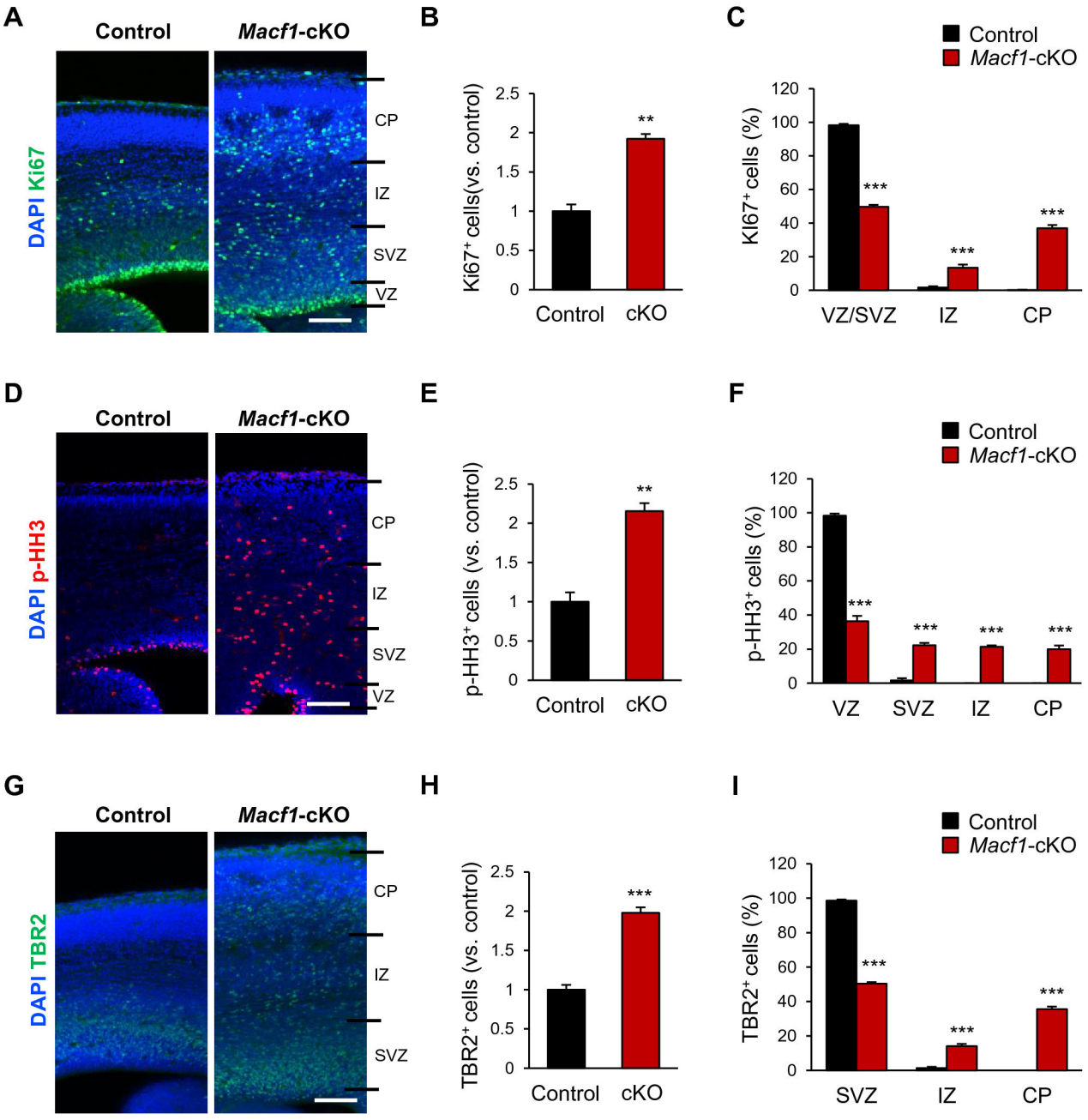

Fig. 4. Increased proliferation of cortical progenitors in *Macf1*-cKO brains

(**A**, **D** and **G**) Cerebral cortices from E14.5 control and *Macf1*-cKO mice were immunostained with an anti-Ki67, anti-phospho Histone H3 (p-HH3) or anti-TBR2 antibody. CP: cortical plate; IZ: intermediate zone; SVZ: subventricular zone; VZ: ventricular zone. Scale bars: 100 μm. (**B**, **E** and **H**) Ki67, phospho-Histone H3, or TBR2-positive cells were quantified in control and *Macf1*-cKO brains. N= 5 mice for each condition. Statistical significance was determined by two-tailed Student's t-test. Data are shown as relative changes versus controls. $^{**}p < 0.01$, $^{***}p < 0.001$. (**C**, **F** and **I**) Quantification of Ki67, phospho-Histone H3, or TBR2-positive cells in cortical

subdivisions. N= 5 mice for each condition. Statistical significance was determined by two-way ANOVA with Bonferonni correction test. ***$p < 0.001$ vs. control.

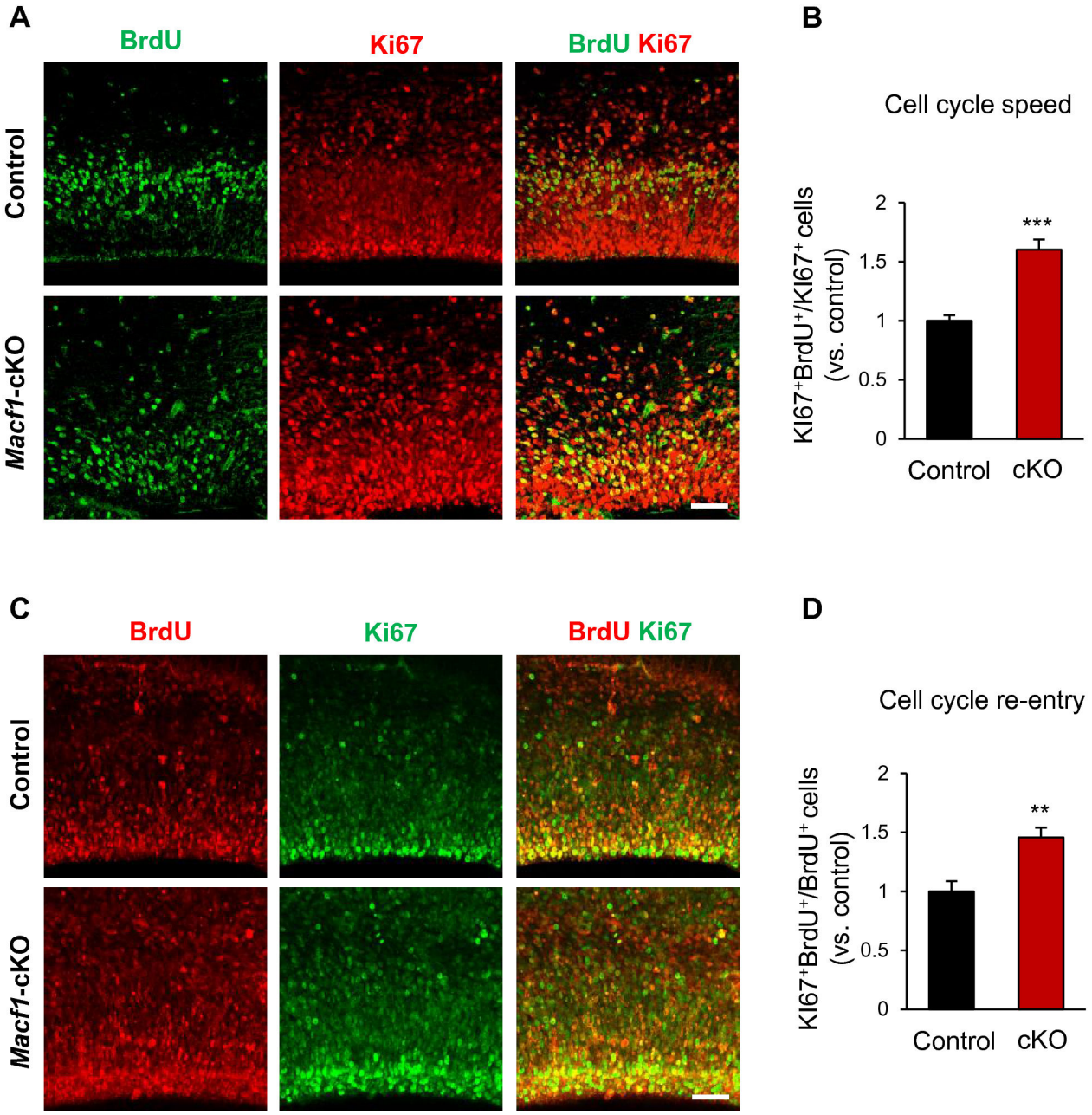

Fig. 5. *Macf1*-cKO cerebral cortices show aberrant cell cycle progression

(**A**) E14.5 control and *Macf1*-cKO mice were pulse-labeled with BrdU for 30 min, and then the cerebral cortex was collected and immunostained using BrdU and Ki67 antibodies. Scale bar: 20 μm. (**B**) Quantification of cell cycle speed. The cell cycle speed was assessed by the fraction of BrdU and Ki67-positive cells in total Ki67-positive cells. N= 5 mice for each condition. Statistical significance was determined by two-tailed Student's t-test. Data are shown as relative changes versus controls. ***$p < 0.001$. (**C**) Double immunostaining to BrdU and Ki67 was performed after a BrdU pulse-labeling of control and *Macf1*-cKO mice for 24 hrs. Scale bar: 20 μm. (**D**) The index of cell cycle re-entry was calculated as the fractions of both BrdU and Ki67-positive cells in total BrdU-positive cells. N= 5 mice for

each condition. Statistical significance was determined by two-tailed Student's t-test. Data are shown as relative changes versus controls. $^{**}p < 0.01$.

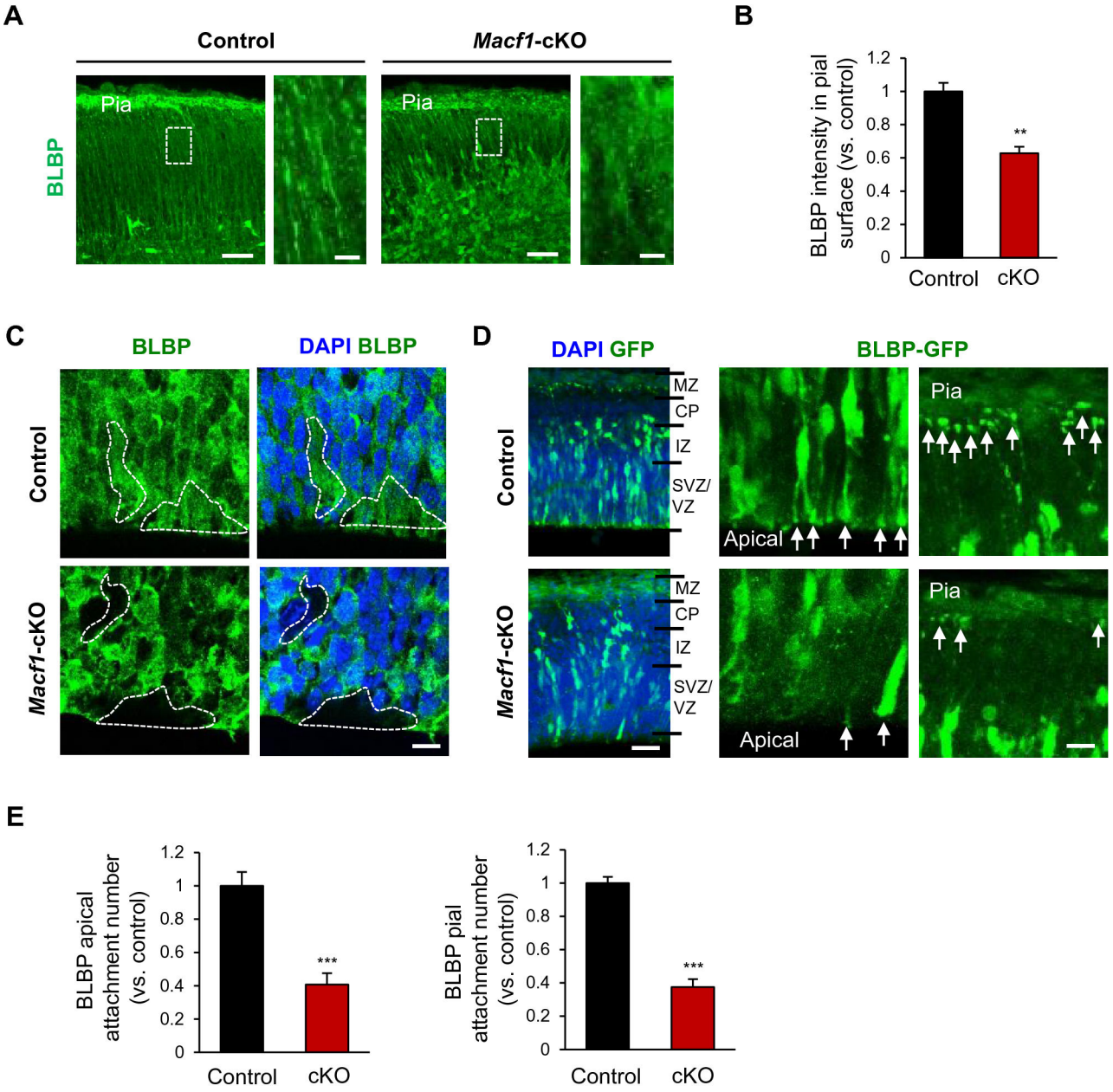

Fig. 6. Apical and basal fiber development is altered in *Macf1*-cKO radial progenitors

(**A**) Radial glial fibers were labeled by BLBP immunostaining in E14.5 control and *Macf1*-cKO cortices. The second and fourth micrographs show higher magnification of dotted rectangular areas in the first and third images. Scale bars: 50 μm (lower magnification), 10 μm (higher magnification). (**B**) Quantifications of BLBP intensity in control and *Macf1*-cKO pial areas. N= 5 mice for each condition. Statistical significance was determined by two-tailed Student's t-test. Data are shown as relative changes versus controls. $^{**}p < 0.01$. (**C**) Higher magnification images of BLBP-immunostained VZs. The tissue sections were counterstained with DAPI. Scale bars: 10 μm. (**D**) E13.5 control and *Macf1*-cKO mice were electroporated *in utero* with a BLBP-EGFP construct to target radial glial progenitors. Electroporated brains were collected after 24 hours. Arrows indicate the end-feet of radial

glial fibers anchoring at the apical or pial surface. MZ: marginal zone. Scale bars: 50 μm (left), 10 μm (right). (**E**) The numbers of attached radial fibers at the VZ or pia were quantified in control and *Macf1*-cKO brains. N= 5 mice for each condition. Statistical significance was determined by two-tailed Student's t-test. Data are shown as relative changes versus controls. ***$p < 0.001$.

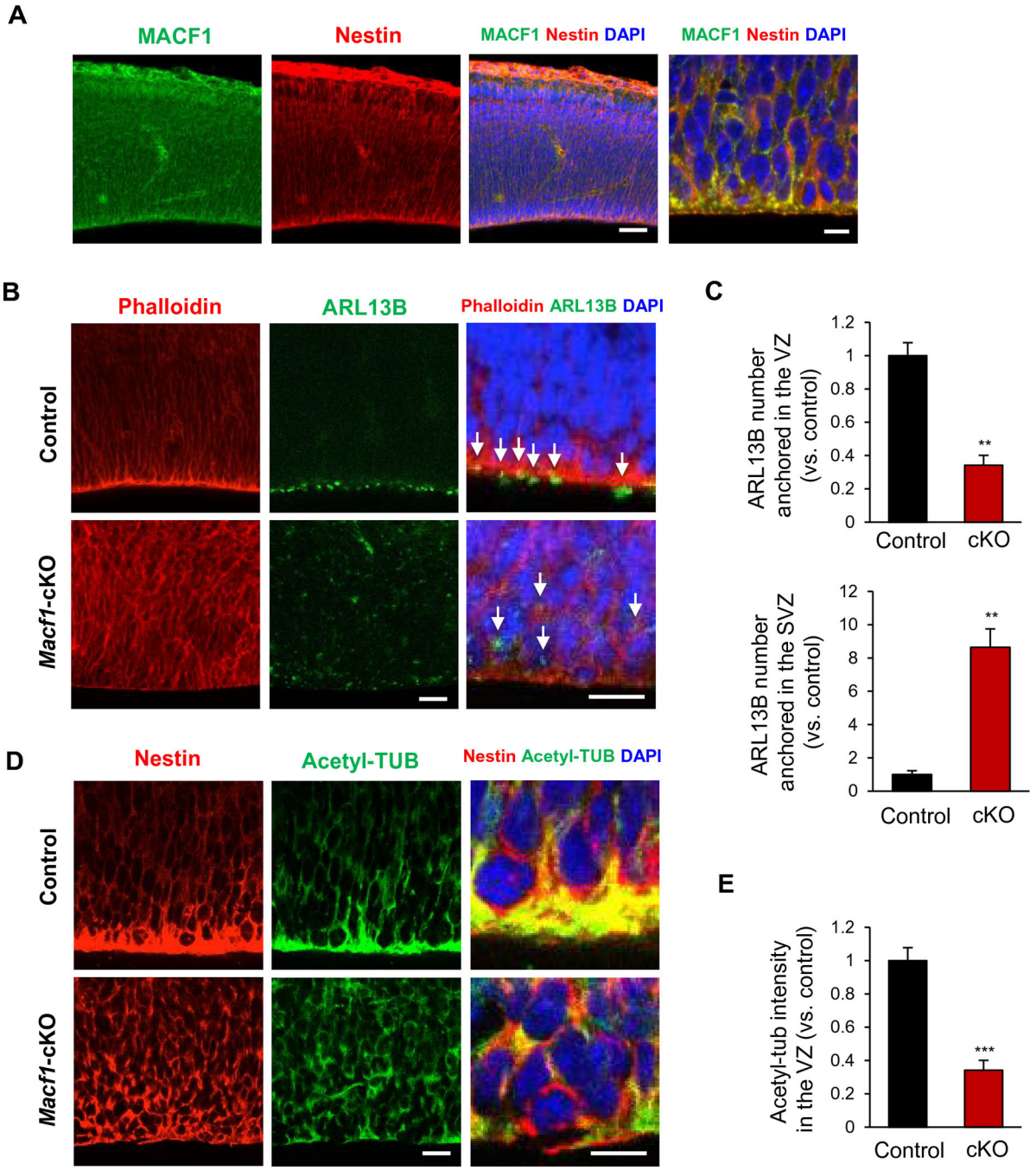

Fig. 7. Cytoskeletal stability and polarity are impaired in the VZ of the *Macf1*-cKO cortex

(**A**) Immunostaining shows MACF1 expression in the cerebral cortex of E14.5 mice. MACF1 was highly expressed in nestin-positive neural progenitors in the VZ. Scale bars: 50 μm (third panel), 10 μm (fourth panel). (**B**) Cerebral cortices from E14.5 control and *Macf1*-cKO mice were immunostained with Phalloidin and an anti-ARL13B antibody. Arrows indicate ARL13B-positive cilia. Scale bars: 20 μm (middle panel), 10 μm (right panel). (**C**) The number of ARL13B positioned in the VZ or SVZ was quantified. N= 5 mice for each condition. Statistical significance was determined by two-tailed Student's t-test. Data are

shown as relative changes versus controls. $^{**}p < 0.01$. (**D**) Cerebral cortices from E14.5 control and *Macf1*-cKO brains were immunostained to acetylated-tubulin and nestin. Scale bars: 20 μm (middle panel), 10 μm (right panel). (**E**) Quantification of acetylated-tubulin at the VZ. N= 5 mice for each condition. Statistical significance was determined by two-tailed Student's t-test. Data are shown as relative changes versus controls. $^{***}p < 0.001$.

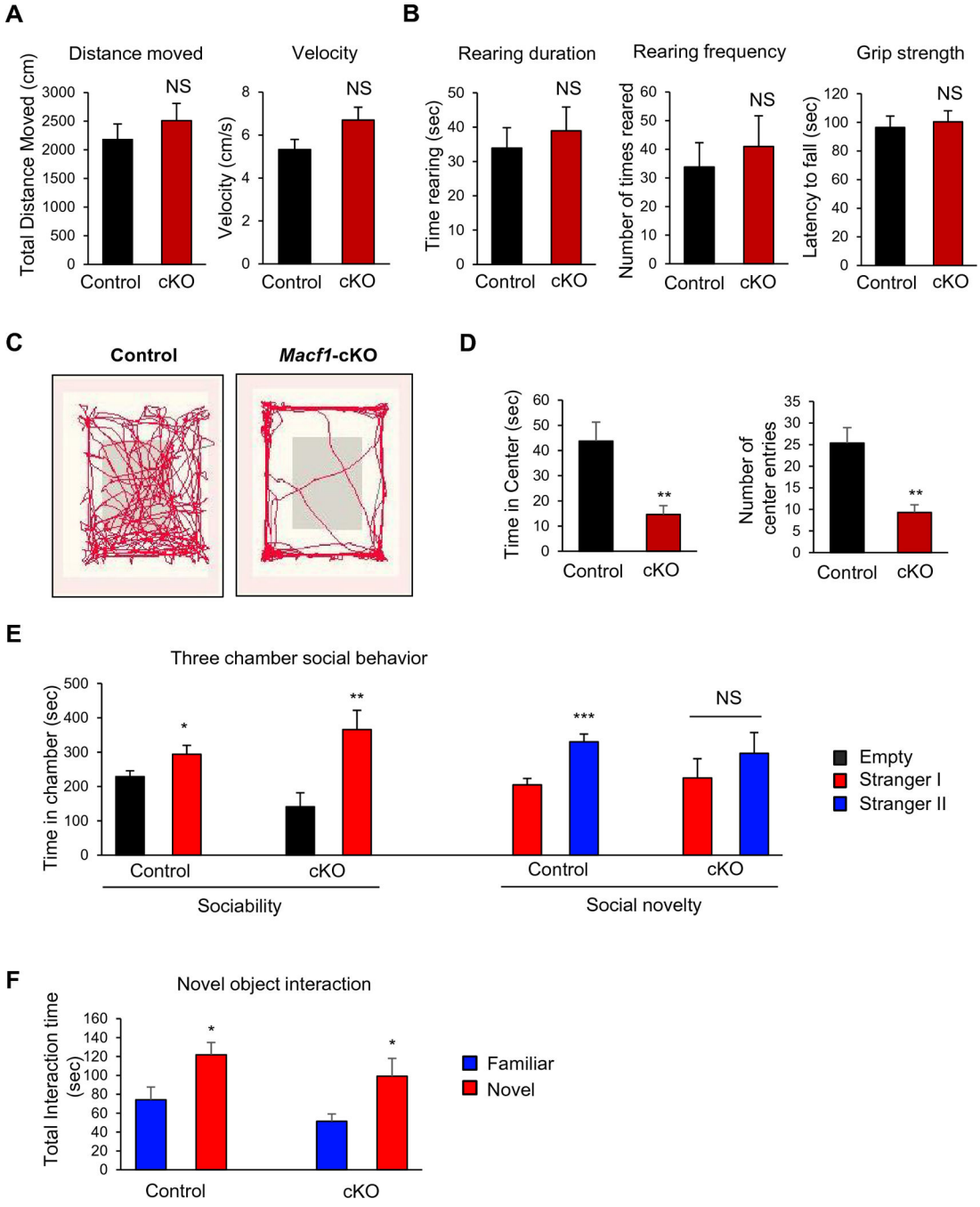

Fig. 8. Anxiety-like behavior and social deficits in *Macf1*-cKO mice

(**A**) Motor activities were assessed by measuring the total distance and mean velocity of movement during the open field test. N= 11 mice for controls and 7 mice for *Macf1*-cKO. Statistical significance was determined by two-tailed Student's t-test. NS: no significance. (**B**) Rearing time and frequency were measured during the rearing test. The grip strength test was also performed to assess the motor activity of *Macf1*-cKO mice. N= 9 mice for controls and 7 mice for *Macf1*-cKO mice. Statistical significance was determined by two-tailed Student's t-test. (**C**) Representative traces of control and *Macf1*-cKO mice in the open field

test. (**D**) Total time spent in the center and the number of entries into the center were quantified in the open field test. N= 11 mice for controls and 7 mice for *Macf1*-cKO mice. Statistical significance was determined by two-tailed Student's t-test. **P < 0.01 versus control. (**E**) The three-chamber social test assessed social behaviors including sociability and social novelty in control and *Macf1*-cKO mice. N= 9 mice for control and 7 mice for *Macf1*-cKO mice. Statistical significance was determined by one-way ANOVA with Bonferonni correction test. *P < 0.05, **P < 0.01, ***P < 0.001 versus empty or stranger I condition. (**F**) The novel object test showed no difference in spatial recognition between controls and *Macf1*-cKO mice. N= 9 mice for controls and 7 mice for *Macf1*-cKO mice. Statistical significance was determined by one-way ANOVA with Bonferonni correction test. *P = 0.05.

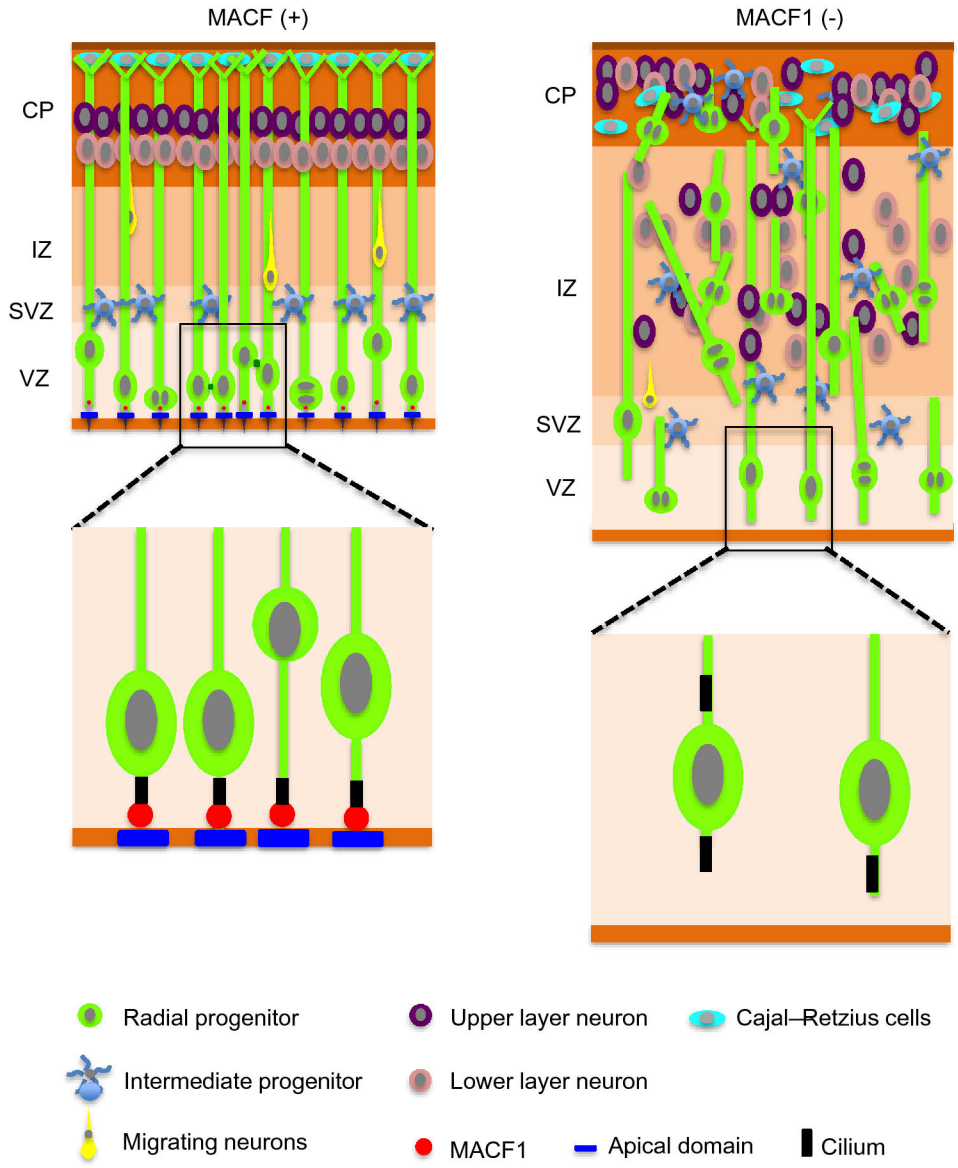

Fig. 9. Model of cortical malformation and SBH in *Macf1*-cKO

MACF1 is required for normal localization of neural progenitors and neurons in the developing cerebral cortex. This tight positioning relies on radial glial stability and polarity, which enables their apical and basal fibers to anchor at the VZ and pia appropriately. MACF1 deficiency alters cytoskeletal stability and polarity leading to ectopic progenitor positioning and SBH as well as neuronal lamination defects.

Table 1.

Materials used in the analysis performed in this work

Antibodies	Use	Details
NeuN	IHC, pan-neuronal	EMD Millipore, MAB337
L1	IHC, cortical axon	EMD Millipore, MAB5272
TBR1	IHC, lower layer neuron	Abcam, ab31940
CUX1	IHC, upper layer neuron	Santa Cruz, sc-13024
MAP2	IHC, pan-neuronal	Abcam, ab5392
GFAP	IHC, astrocyte	Abcam, ab7260
Ki67	IHC, actively proliferating cell	Cell Signaling, #9129
phospho-Histone H3	IHC, mitotic cell	Cell Signaling, #9701S
BrdU	IHC, S-phase cell	BD Biosciences, 555627
Tbr2	IHC, intermediate progenitor	EMD Millipore, ab15894
BLBP	IHC, radial fiber	Abcam, ab32423
Nestin	IHC, radial progenitor	PhosphoSolutions, 1435-NES
ARL13B	IHC, cilia	Abcam, ab83879
Acetyl-α-Tubulin	IHC, stable microtubule	Cell Signaling, #5335
GFP	IHC	Thermo Fisher, A11122, A10262
MACF1	IHC	Santa Cruz, sc-377532
AlexaFluor568-Phalloidin	IHC, polymerized actin	ThermoFisher, A12380